

# Application of Ray Tracing for Interpreting Beam Prints from the Fibre Laser Cutting of Stainless Steel

M. ALOTAIBI<sup>1,2</sup>, H. ATIYAH<sup>1</sup>, R.C.I. MACKENZIE<sup>1</sup>  
AND K.T. VOISEY<sup>1,\*</sup>

<sup>1</sup>*Faculty of Engineering, University of Nottingham, University Park,  
Nottingham, NG7 2RD, UK*

<sup>2</sup>*Electrical Engineering Department, Faculty of Engineering,  
Taibah University, Madinah 42353, Saudi Arabia*

Two-dimensional (2-D) ray tracing has been used to investigate the influence of inclined cutting front and the cutting edge on the exiting, surplus, laser beam while cutting 6 mm thick stainless steel sheet with a 1070 nm wavelength fibre laser. The ray tracing model, which assumed a Gaussian beam, has investigated the distribution of this surplus beam as a function of kerf wall inclination angle. Multiple reflections are shown to broaden the spatial distribution of the surplus beam. Dross and kerf wall roughness also broaden the spatial distribution of the surplus beam. Comparison of an experimentally obtained beam print from the surplus beam for 1070 nm fibre laser cutting of 6 mm thick stainless steel with modelled results allows inclination of the cut front to be estimated. The experimentally obtained beam print has features consistent with roughness/dross induced beam broadening.

*Keywords: Fibre laser, 304L stainless steel, black poly(methyl methacrylate) (PMMA), laser cutting, beam print, surplus energy, ray tracing, two-dimensional (2-D) ray tracing, simulation*

## 1 INTRODUCTION

Fibre lasers are widely used in many industrial sectors, from dental to automotive fabrication, for materials processing and in particular for non-contact cutting applications. Fibre laser cutting is preferred over other laser systems

---

\*Corresponding author: Tel: +44 (0)115 951 4139; E-mail: katy.voisey@nottingham.ac.uk

due to good wall plug efficiency and high brightness as well as superior cut quality for thin sheet cutting [1].

There is a body of work on the efficiency of the actual laser cutting process, this focusses on using a power balance approach to determine the proportion of incident energy that is directly utilized in laser cutting [2-4]. As has been previously reported [5, 6], the efficiency varies with cutting speed. At low and moderate cutting speeds a portion of the laser beam passes through the cut without interacting with the material. It is also known that a portion of the laser beam reflects off the material and exits the bottom of the cut zone. The slope of the cut front also varies with cutting speed, being near vertical at low speeds and more inclined at higher cutting speeds [5].

With a better understanding of the interaction between the incident laser beam and the cutting surface, and the surplus energy (the proportion of the laser beam that is not directly involved in the cutting process), more energy efficient cutting strategies can be designed. This paper uses ray tracing to investigate the surplus energy in fibre laser cutting of stainless steel.

## **2 EXPERIMENTAL MATERIALS, APPARATUS AND PROCEDURES**

A multimode 2 kW, 1070 nm wavelength fibre laser (YLR-2000; IPG Photonics Corporation) was used in the continuous wave (CW) mode. A laser power of 1850 W was used to cut 6 mm thick stainless steel 304L at 729 mm/min, 95% of the maximum cutting speed. The fibre laser beam was delivered *via* a 200  $\mu\text{m}$  diameter delivery beam into a cutting head, then focussed with a 120 mm focal length lens into a 192  $\mu\text{m}$  spot on the top surface of the stainless steel. The full angle divergence of this focussed beam was 0.153 rad. A 1 mm diameter nozzle 1 mm above the sample surface was used to deliver the assist gas coaxially to the laser beam.  $\text{N}_2$  was used as an assist gas with pressure 13 bar.

To investigate the 2-D surplus energy distribution a black poly(methyl methacrylate) (PMMA) collection sheet was positioned 17.5 mm below the bottom of the workpiece. Any fibre laser radiation exiting the bottom of the cut would, therefore, be absorbed by the black PMMA block. Since absorption of the laser radiation by the black PMMA results in material removal, the surplus energy distribution can be determined by examining the shape of the cavity on the surface of the black PMMA.

It is important to note that during cutting the laser and black PMMA block remained stationary while the stainless steel sheet was translated between them. This ensured that the cutting front position was stationary with respect to the black PMMA block, allowing the 2-D surplus energy distribution corresponding to steady state cutting to be studied. In order to ensure that only surplus energy from steady state cutting at the selected speed was collected,

an additional piece of stainless steel was fixed below the main cutting sheet block the path to the black PMMA during the time that the translation table was accelerating.

### 3 SIMULATION METHODOLOGY

A 2-D ray tracing code was developed using MATLAB. In order to use this 2-D model the three-dimensional (3-D) cut kerf geometry has been simplified: the cut front and kerf walls have been considered as straight inclined lines (see Figure 1). The cut front curvature is not included in this work.

The real, experimental, laser beam had a full angle divergence of 0.153 rad and was focussed to a 200  $\mu\text{m}$  diameter spot at the sample surface. This was simulated by firing 500,000 photons of unit energy from a point 1.3 mm above the surface so that the beam had diverged to a 200  $\mu\text{m}$  spot at the surface (see Figure 2). The direction of each photon was determined by using random numbers, generated using the `randn` MATLAB function, that are normally distributed across the 0.153 rad range. This is equivalent to assuming the beam had a Gaussian beam profile. This is an approximation as the real beam has an  $M^2$  value of 23.3 and is therefore not a perfect Gaussian.

In this model specular reflection has been assumed. Fresnel reflection and absorption equations were used to determine the extent of absorption at each reflection as function of the angle of incidence. The refractive index of melted iron was obtained from [7, 8] and substituted into the Fresnel equation. Each photon was ray traced until it either reached the collection sheet or its energy dropped below 1% of its initial energy or it was reflected back towards the source. The collection sheet represents the black PMMA and is located in a plane 17.5 mm beneath the workpiece, as shown in Figure 2. The location and energy of each photon reaching the collection sheet was recorded and presented as an intensity profile.

Two types of simulation have been run: cut front; and kerf walls. The cut front simulations have a single piece of material (see Figure 2(a)) and simulate energy redistribution along the direction of the cut. The kerf walls simulations include the two kerf walls (see Figure 2(b)) and simulate energy

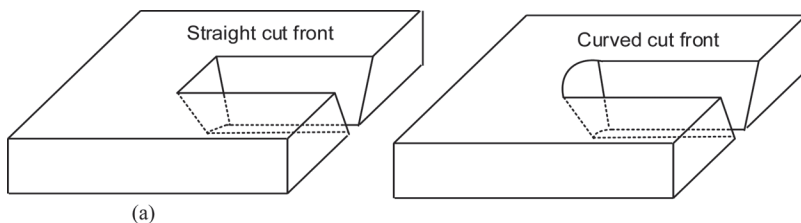


FIGURE 1

Schematic diagrams of (a) the assumed straight cut front and (b) the real curved cut front.

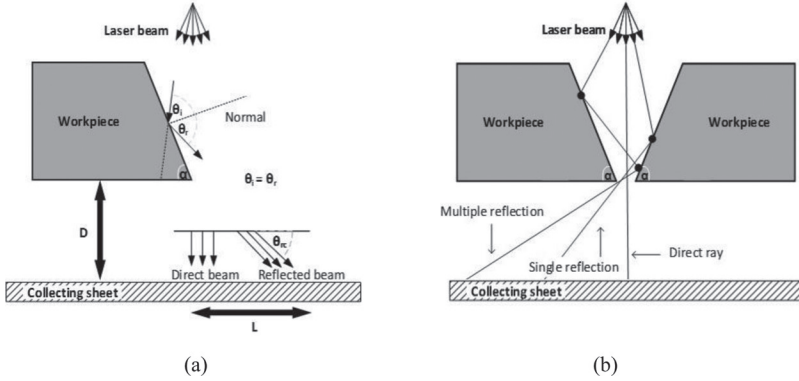


FIGURE 2  
Schematic diagrams of the two 2-D ray tracing simulations run for (a) simulation of the cut front and (b) simulation of the kerf walls.

redistribution perpendicular to the cut direction. Intensity profiles have been determined for different cut front and kerf wall inclinations.

All the intensity profiles presented show the sum of the intensity of all photons reaching the collecting plane through the 6 mm workpiece thickness and 0.31 mm bottom kerf width, unless otherwise specified. The width of each bin in the histograms is 0.10 mm and zero on the distance axis denotes the centre line of the beam

A pseudo 2-D intensity profile was obtained by combining results from cut front and kerf wall simulations. This was obtained by treating the intensity profile generated by the cut front as a row matrix and multiplying this by a column matrix representing the modelled kerf wall intensity distribution.

## 4 RESULTS AND DISCUSSION

### 4.1 Cut front simulation

The effect of cut front inclinations is shown in Figure 3. The laser beam was centred on the bottom edge of the workpiece. It can be seen that an inclined cut front splits the laser beam into two parts. Of these, the first part passes directly through the cut and reaches the collecting plane with no losses. The second part reflects off the cut front, the partial absorption during this interaction decreases the intensity of these reflected photons.

The overall spread of the collected intensity distribution,  $L$  (*cf.* Figure 2), the maximum distance from the origin at which photons are detected, can be determined *via* geometry:

$$L = (D + h) \tan(\pi + \theta_{d/2} - 2a) - (x + b_{d/2}) \quad (1)$$

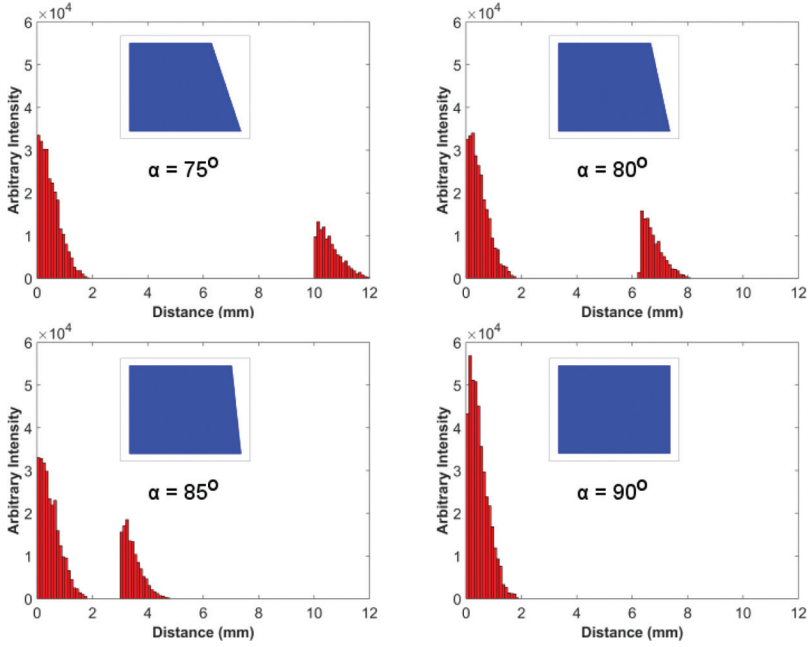


FIGURE 3  
Intensity profiles for different cut front inclinations.

where  $a$  is the cut front inclination,  $b_{d/2}$  is the laser beam radius at the sample surface,  $\theta_{d/2}$  is the half angle divergence,  $D$  is the distance between the base of sample and the collecting sheet,  $h$  is the height above base of the sample where edge of the laser beam meets the cut front and  $x$  is the horizontal offset between the laser beam edge at the sample surface and where it meets the cut front. To determine  $L$ , two other distances,  $h$  and  $x$  must first be determined. As can be seen from Figure 4:

$$\tan a = \frac{h}{x + b_{d/2}} \quad (2)$$

and

$$\tan \theta_{d/2} = \frac{x}{t - h} \quad (3)$$

where  $t$  is material thickness. Now, we can combine Equation (2) and Equation (3) and solve for  $x$ :

$$x = \frac{t - b_{d/2} \tan a}{\tan a + \frac{1}{\tan \theta_{d/2}}} \quad (4)$$

TABLE 1

Comparison of calculated and modelled values for the extent of the energy distribution.

Cut Front Inclination, $a$ ( $^{\circ}$ )	$L_{\text{calc}}$ (mm)	$L_{\text{model}}$ (mm)
75	12.70	12.00
80	8.50	8.00
85	5.10	4.80

The expression for  $x$  in Equation (4) can then be substituted back into Equation 2 and rearranged to give  $h$ . The overall expression for  $L$  can now be utilized.

Table 1 shows both calculated and modelled values of  $L$  as a function of cut front inclination. It is clear that for the set up studied here that the cut front inclination angle has a measureable effect on  $L$ , the spread of the intensity distribution. There is good correlation between the calculated and modelled results, with the modelled results being consistently about 3% lower.

#### 4.2 Kerf walls simulation

For these simulations, the laser beam was centred on the midpoint of the bottom kerf. Figure 5 shows the intensity profiles for different cut edge inclinations and kerf widths.

For kerf wall inclinations up to  $45.0^{\circ}$ , photons either pass straight through the kerf, and reach the collection plate with their original intensity, or are reflected upwards and exit the system through the top of the kerf and so never reach the collection plate. Hence the intensity profiles for kerf wall inclinations of  $30.0^{\circ}$  and  $45.0^{\circ}$  are essentially identical, they have the same  $L$  value and the slight differences in the shape of the central peak are attributed to the process of using randn to determine the direction of each specific photon.

For kerf wall inclinations greater than  $45.0^{\circ}$  distinct side lobes with lower intensities than the main peak are detected. The main peak again corresponds to the portion of the beam that passes directly through the kerf without interacting with the material. The other portions of the beam are of decreased intensity because they have undergone reflection and hence had their intensity reduced by partial absorption during reflection. As the inclination angle increases, the separation between the side lobes and the main peak decreases.

Narrowing the cutting kerf by half for  $80.0$  and  $85.0^{\circ}$ , as illustrated in Figure 4, widens the energy distribution. As discussed by Petring *et al.* [9] the angle of incidence is progressively decreased by multiple reflections within the cutting channel. As well as increasing the extent of absorption at each reflection this results in an increased angular spread of photons exiting the bottom of the cut, producing a larger spread in the detected energy distribution at the collection plate.

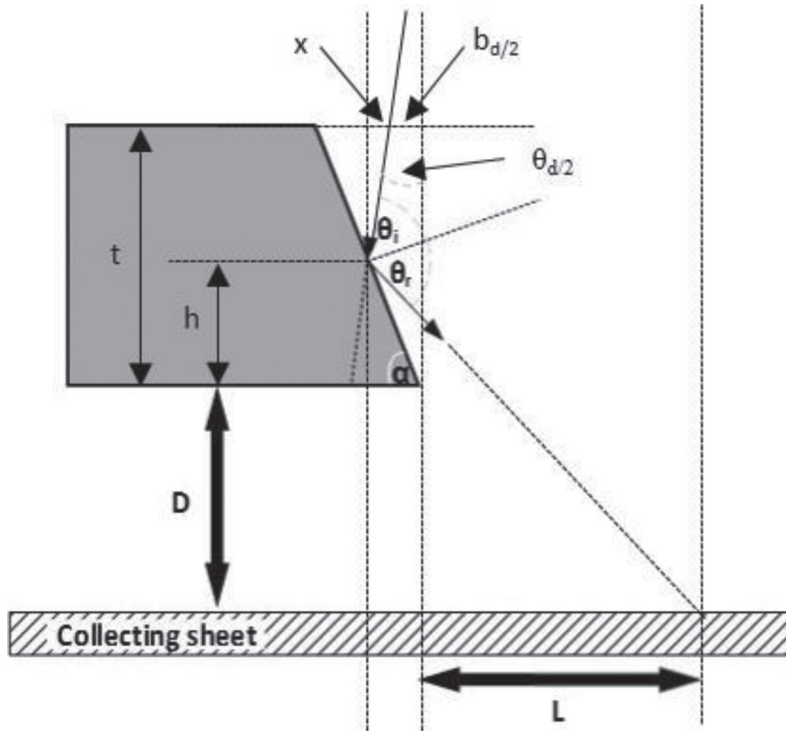


FIGURE 4  
Cut front geometry details used to calculate  $L$ .

### 4.3 Kerf wall roughness effect

Real kerf geometries were extracted from metallographic cross-sections and imported into the model (see Figure 6). It must be noted that these cross-sections show the final surface of the kerf walls and that this is not necessarily the same as a snap shot view of the roughness that existed during the cutting process; nevertheless, it is clear that the assumption of flat kerf walls, and cut front, is not correct.

Figure 6 shows the modelled intensity profile obtained from the real cross-section. The presence of roughness has resulted in a spread in the intensity distribution. As for the intensity distributions shown in Figure 5, this spread is attributed to multiple reflections within the kerf. The irregularity of the real surface has produced an irregular intensity distribution. The central, straight-through, peak is still clear however the distinct side lobes have now disappeared, being replaced with a less distinct, irregular intensity profile.

To investigate the effect of the kerf wall roughness, a single bump was attached to one side of the wall. The effect of the position of this bump on the collected intensity distribution is seen Figure 7. The presence of the bump

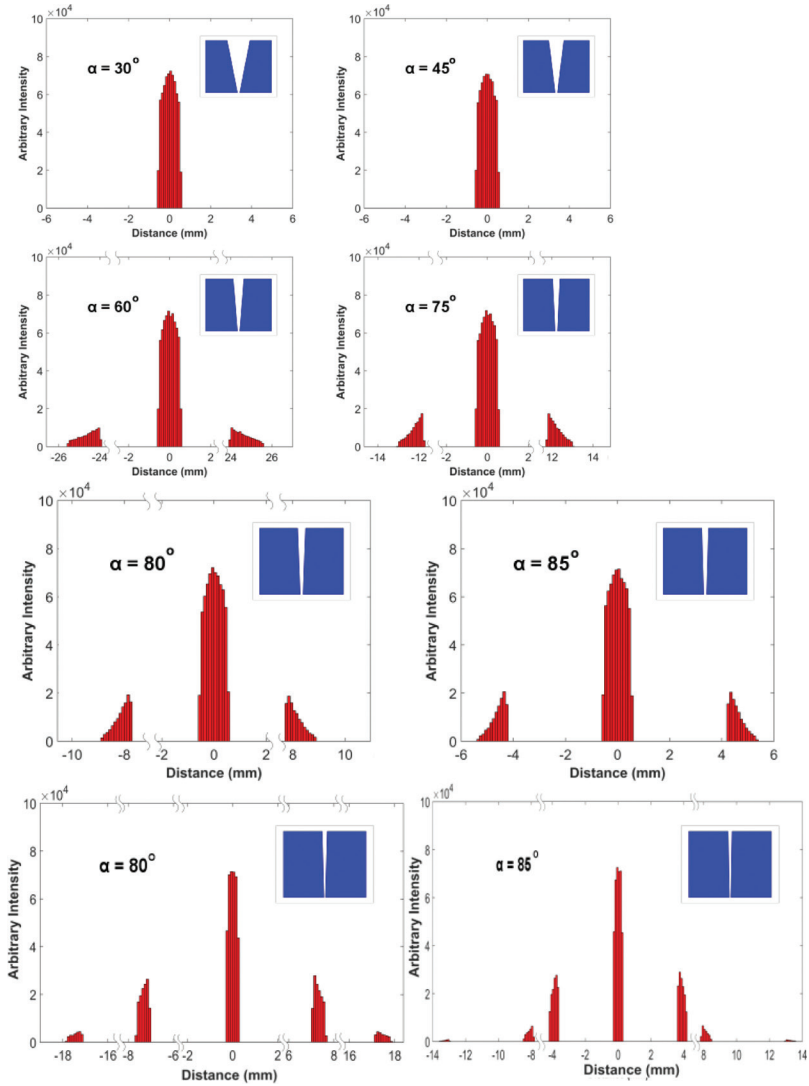
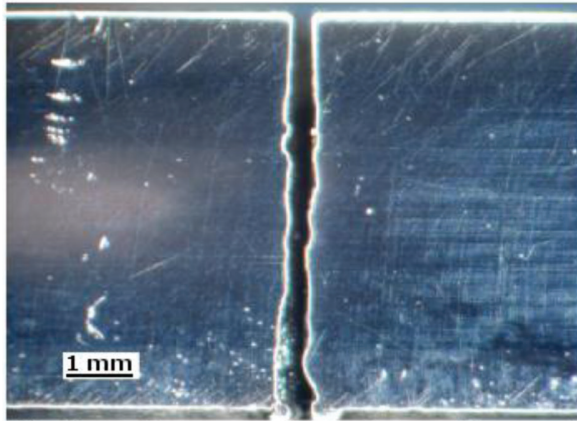


FIGURE 5

Intensity profiles for different kerf wall inclinations. Note the discontinuity in the x-axis for the two profiles in the bottom row.

increases the spread of the intensity distribution, and decreases the size of the central peak. It is seen that nearer the bump is to the top of the kerf the greater the effect it has. This can be understood by considering the ray diagram in Figure 8, after the bump is hit the angle of incidence is first dramatically changed and then more progressively decreased by multiple reflections within the cutting channel as discussed by Petring *et al.* [9]. The higher up the cut this happens the more extensive the change in angle of incidence will be, and



**Metallographic cross section for 6mm stainless steel**

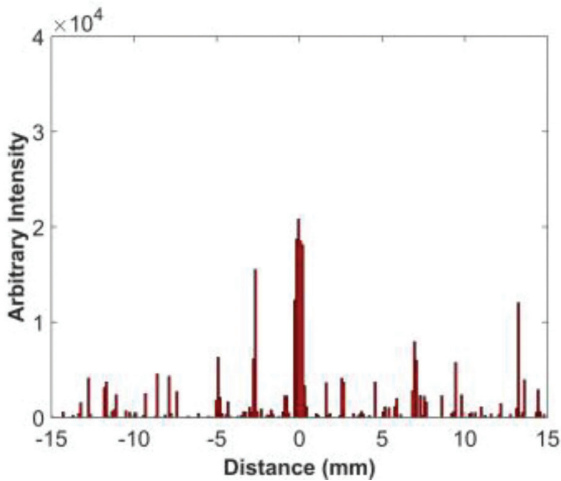


FIGURE 6

Optical micrograph of the cross-section of real cut (upper) and corresponding modelled collected intensity distribution (lower).

hence when the photons exit the cut they will be dispersed through a larger range of angles.

Figure 6 shows some adherent dross at the bottom of the kerf, the effect of dross has also been modelled. Circular features representing dross were added to the bottom of the cut edge, with the centre point of the circular dross centred on the bottom corners of the kerf walls (see Figure 9).

Figure 10 shows that the presence of dross modifies the modelled collected intensity profile. The lateral spread of the profile increases and the width of the straight-through peak decreases as part of it becomes blocked by the dross. Asymmetrical dross results in asymmetry in the collected intensity profile.

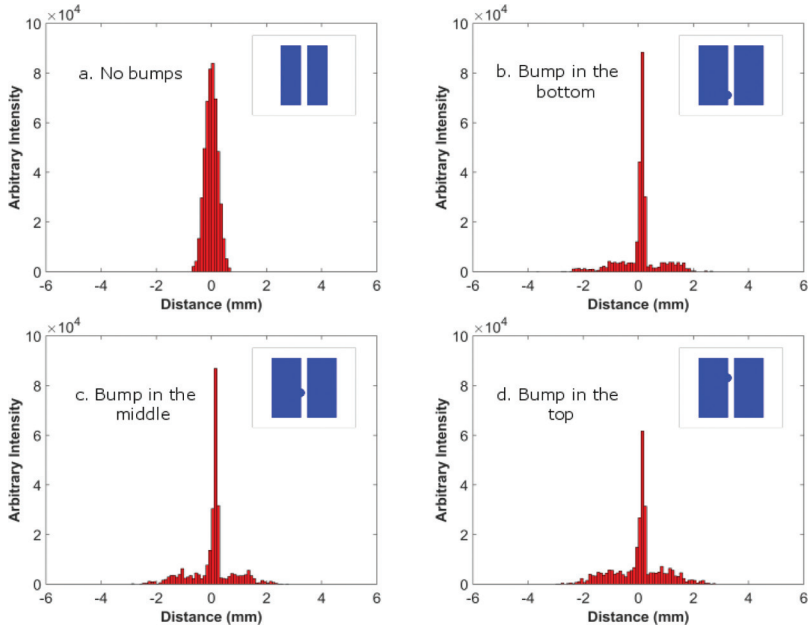


FIGURE 7  
Intensity profiles for kerf walls with different bumps. All bumps radius = 0.10 mm.

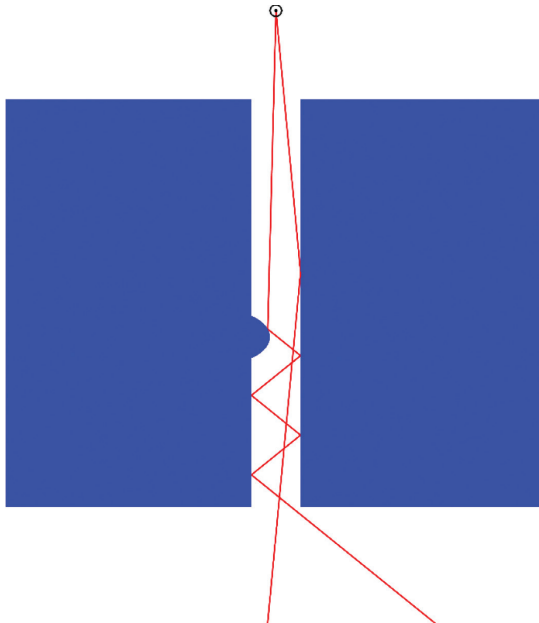


FIGURE 8  
Ray tracing diagram showing effect of bump on path of photon through cut kerf.

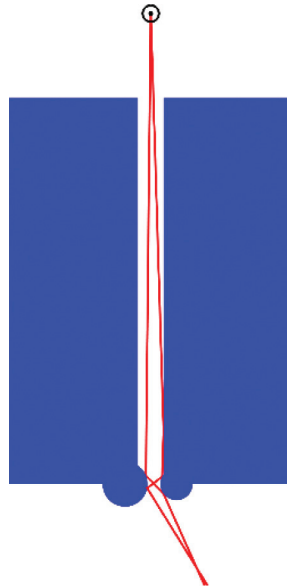


FIGURE 9  
Ray tracing diagram showing effect of dross on path of photons through cut kerf.

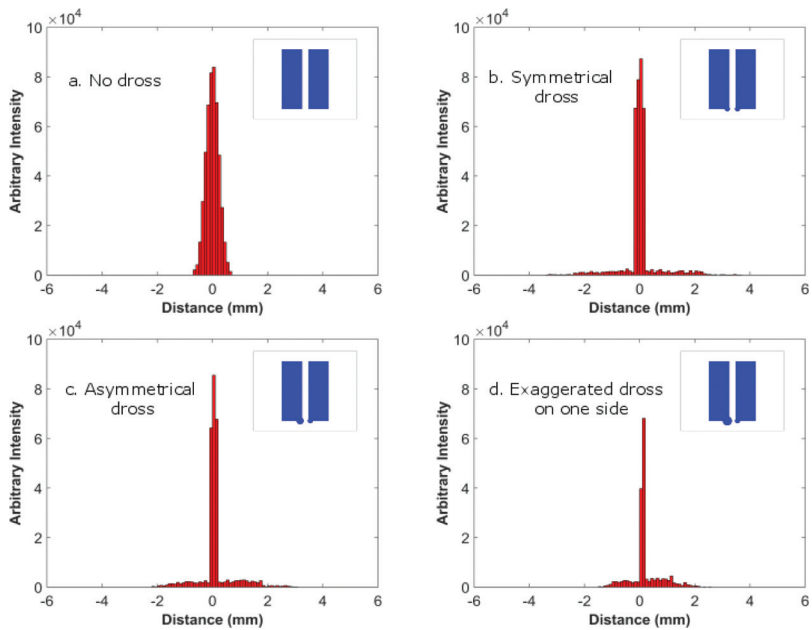


FIGURE 10  
Intensity profile as a function of dross.

## 5 COMPARISON OF MODELLED AND EXPERIMENTAL RESULTS

Figure 11 shows experimentally obtained and modelled 2-D surplus energy distributions. The relationship between lateral extent of the intensity profile generated by the cut front and cut front inclination angle was shown earlier (*cf.* Equation (1)). The 2-D surplus energy distribution shown below was generated using a cut front inclination of  $66.0^\circ$ . The good match in lateral extent of the two distributions could be taken to indicate that this is the actual cut front inclination. Still, this inclination is not as large as would be expected from the published literature on fibre laser cutting [5].

It must be noted that the modelled 2-D energy distribution did not include any effects of dross or roughness of the cut front, effects which results presented above show would increase the spread of the energy distribution;

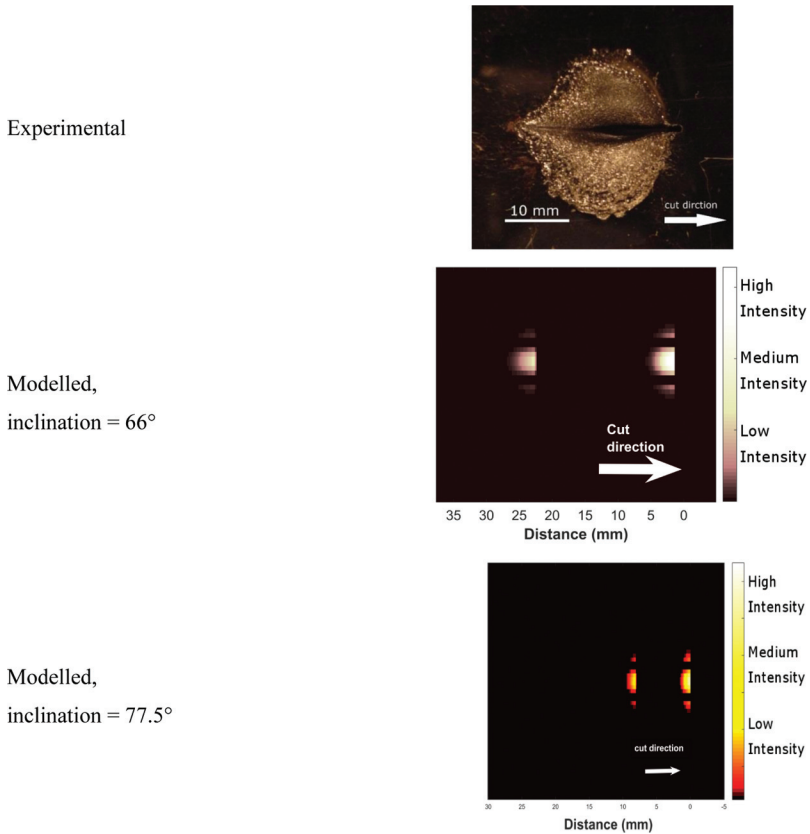


FIGURE 11  
Experimental (top) and modelled (middle and bottom) 2-D surplus energy distributions, presented at the same magnifications.

hence it is not appropriate to attempt to match the extent of spread of the energy distribution here and a different approach is required.

Examination of the experimental profile clearly shows a main, central, region starting with the straight through beam, then broadening to a maximum after approximately 10 mm. This is will be the location of the beam reflected from the cut front. The modelled 2-D surplus energy distribution has been regenerated to take this into account. It was found that a cut front inclination of  $77.5^\circ$  placed the main reflected beam in the same region as the broadest point of the central part of the experimental surplus energy distribution. This is in line with previously published reports of cut front geometry [5]. The remaining area of the experimental 2-D surplus energy distribution; that is, the area that extends approximately 10 mm from the main central region, is attributed to the effect of roughness producing a large spread in the directions of photons exiting the cut. This is consistent with the geometry of this region, which is symmetrical about the cut line, due to the two sides of the kerf but extending only rearwards, away from the cut front along the cut line since in this direction there is only the cut front with no rear wall to generate multiple reflections.

## 6 CONCLUSIONS

In this study a two-dimensional (2-D) ray tracing model has been written in MATLAB and applied to fibre laser cutting of mild steel. The model has been validated *via* comparison with geometrical analysis. This work has demonstrated:

- (i) How cut front inclination affects the main reflected beam;
- (ii) That kerf wall inclination can generate multiple reflections which broaden the spatial spread of surplus energy;
- (iii) The importance of dross and roughness in broadening the spatial spread of surplus energy, with the effect of roughness being more significant the nearer the top of the cut it occurs; and
- (iv) The significant differences between modelled and experimentally obtained 2-D surplus energy distributions are attributed to the roughness of the cut front and kerf walls.

## NOMENCLATURE

$a$	Cut front inclination (degrees)
$b_{d/2}$	Laser beam radius at the sample surface (m)
$D$	Distance between the base of the sample and the collecting sheet (m)

$h$	Height above base of the sample where the edge of the laser beam meets the cut front (m)
$L$	Spread of intensity distribution (m)
$t$	Sample thickness (m)
$x$	Horizontal offset between the laser beam edge at the sample surface and where it meets the cut front (m)

### Greek symbol

$\theta_{d/2}$	Half angle divergence (degrees)
----------------	---------------------------------

### REFERENCES

- [1] Mullick S., Shrawgi S., Kangale A., Agrawal A. and Nath A. Effects of fibre laser beam focal point location and incidence angle on the cut quality of stainless steel sheet. *Lasers in Engineering* **36**(1-3) (2017), 3–30.
- [2] Scintilla L.D., Tricarico L., Wetzig A., Mahrle A. and Beyer E. Primary losses in disk and CO<sub>2</sub> laser beam inert gas fusion cutting. *Journal of Materials Processing Technology* **211**(12) (2011), 2050–2061.
- [3] Scintilla L.D., Tricarico L., Wetzig A. and Beyer E. Investigation on disk and CO<sub>2</sub> laser beam fusion cutting differences based on power balance equation. *International Journal of Machine Tools and Manufacture* **69** (2013), 30–37.
- [4] Pocorni J., Powell J., Deichsel E., Frostevarg J. and Kaplan A.F.H. Fibre laser cutting stainless steel: Fluid dynamics and cut front morphology. *Optics & Laser Technology* **87** (2017), 87–93.
- [5] Powell J, Al-Mashikhi S.O., Kaplan A.F.H. and Voisey K.T. Fibre laser cutting of thin section mild steel: an explanation of the ‘striation free’ effect. *Optics and Lasers in Engineering* **49**(8) (2011),1069–1075.
- [6] Steen W.M. *Laser Material Processing*. London: Springer-Verlag. 2003.
- [7] Mahrle A., Bartels F. and Beyer E. Theoretical aspects of the process efficiency in laser beam cutting with fiber lasers. *The 27<sup>th</sup> International Congress on Applications of Lasers and Electro Optics (ICALEO 2008)*. 20-23 October 2008, Temecula, CA., USA. pp. 703–712.
- [8] Petring D., Schneider F., Wolf N. and Nazery V. The relevance of brightness for high power laser cutting and welding. *The 27<sup>th</sup> International Congress on Applications of Lasers & Electro-Optics (ICALEO-2008)*. 20-23 October 2008, Temecula, CA., USA. pp. 95–103.
- [9] Petring D. Virtual laser cutting simulation for real parameter optimization. *The 84th Laser Materials Processing Conference*. 19-20 January 2016, Nagoya, Japan. pp. 11–18.